IEEE Access
Multidisciplinary ⋮ Rapid Review ⋮ Open Access Journal

Received 7 December 2022, accepted 30 December 2022, date of publication 9 January 2023, date of current version 17 January 2023.

Digital Object Identifier 10.1109/ACCESS.2023.3235408

RESEARCH ARTICLE

Model Validation of Synchronous Motors With a New Standstill Measurement Technique

ANDREA CREDO[1], ILYA PETROV[2], VALERII ABRAMENKO[2], AND JUHA PYRHÖNEN[2], (Senior Member, IEEE)

[1]Department of Industrial and Information Engineering and Economics, University of L'Aquila, 67100 L'Aquila, Italy
[2]School of Energy Systems, Lappeenranta University of Technology, 53851 Lappeenranta, Finland

Corresponding author: Andrea Credo (Andrea.Credo@univaq.it)

This work was supported by the Academy of Finland's Centre of Excellence in High-Speed Energy Conversion Systems.

ABSTRACT Permanent magnet synchronous machines (PMSM), synchronous reluctance machines (SynRM), and electrically excited synchronous machines (EESM) are widely used in the industry and transportation sectors. Their rotors are often equipped with conducting parts like permanent magnets, thick rotor laminations, damper windings, or a conducting sleeve, or they even have a solid rotor core. Such conducting elements do not allow applying standard AC supply techniques for inductance measurements because of the alternating flux induced by eddy currents. We propose a new technique for inductance measurement at a standstill with a quasi-static voltage supply, which mitigates the eddy current phenomenon. The inductance is measured at several rotor positions over a complete electrical cycle, which allows to proceed with a harmonic spectrum analysis of the inductance variation. With this information, it is possible to estimate motor performance characteristics, such as optimum torque, voltage control, power factor, and torque ripple. The new technique is experimentally validated on a 12 kW axially laminated anisotropic solid-rotor high-speed SynRM. In principle, the method also suits PMSMs, EESMs, and other synchronous machines (not verified in this paper). Experimental validation with a solid-rotor SynRM shows a good correspondence with the simulation. Furthermore, the torque computed using the measured inductance is very similar to the experimental one confirming the effectiveness of the method.

INDEX TERMS ALASynRM, axially laminated anisotropic rotor, high efficiency, high speed, inductance harmonics, inductance measurement, solid rotor, space harmonics, torque harmonics.

I. INTRODUCTION

Synchronous machines (SM) avoid slip-related rotor losses, which are always present in induction machines (IM). In addition, SMs can use different means to improve the power factor and efficiency of the electric motor drive. To obtain optimized characteristics for SMs, extensive optimization algorithms can be used [1], [2], [3], [4]. In order to verify the results of the optimization sequence, a proper measurement procedure is required. The results are affected by manufacturing tolerances and deviations of material properties, which can be considered with robust optimization techniques [5], [6], [7]. Typically, a standard electrical machine test setup comprises a load machine, a torque transducer, and a power analyzer [8], [9]. With such a test setup, efficiency, thermal management, power factor, and voltage and current waveforms can be measured. It is, however, challenging or even impossible to precisely measure the torque ripple of a rotating rotor at different current vectors (referred to the rotor reference frame) as well as inductance variations of the machine at different rotor positions (including inductances along the d- and q-axes). For this reason, most of the literature on the analysis of the torque ripple phenomenon does not address actual verification of torque ripple results obtained by measurements [10], [11], [12]. The same applies to exact inductance values of the machine, when the actual average inductance (over a complete electrical period) can be measured either directly only at one current vector angle (e.g., d-axis inductance by magnetizing the machine along the d-axis at no-load) or indirectly at some other current vector angles (e.g., q-axis

The associate editor coordinating the review of this manuscript and approving it for publication was Kan Liu.

inductance when at a certain load the $I_d = 0$ control is ensured), or the simulation results are not verified at all [13]. However, it was shown in [14] that the actual inductance variation (which can significantly deviate from the average inductance value) as a function of rotor position can affect the torque ripple and can even impair the controllability of the machine. Therefore, analysis of the actual inductance values (including its variation as a function of rotor position) is a vital aspect in a proper optimization process of the SM. Consequently, an accurate inductance measurement procedure to verify the simulation results should also be established.

Another traditional approach to measure the inductance of SMs is to use a standstill approach, which allows to adjust and fix any rotor position and measure the inductance variation as a function of rotor position and current vector angle [15], [16]. However, this method is performed with alternating current, which causes an alternating flux in the air gap and the rotor core. Therefore, the method cannot be applied with highly conducting elements on the rotor side, especially when the rotor is made of galvanically non-insulated solid metal components. Furthermore, most of these methods combine power supply circuits with the measurement circuits, which either reduce the precision of the measurements or require expensive high-precision equipment [17].

This paper describes an inductance measurement process for precise inductance measurement of a three-phase SM at different rotor positions. The proposed method does not require installation of extra windings (e.g., excitation winding or sensing winding), and all the measurements are carried out employing the standard three-phase windings that the machine armature already has. Furthermore, the method allows to separate the power supply circuit from the measurement circuit, which enables high precision with reasonable effort. In addition, the paper provides an example of a postprocessing routine for inductance measurement results to compute torque ripple values that are similar to the actual torque ripple of the assembled motor. The analysis method described in the paper can, in principle, be also applied to permanent magnet synchronous machines (PMSMs), electrically excited synchronous machines (EESMs), synchronous reluctance machines (SynRMs), and other types of SMs. For complete investigation of the electromagnetic performance of PMSMs and EESMs, along with inductance measurements, also back EMF measurement is needed, which is a standard procedure and does not require any special approach. In particular, an Axially Laminated Synchronous Reluctance Machine (ALASynRM) is investigated by applying the proposed approach, because its performance is most dependent on correct inductance characteristics.

The method also allows to evaluate permeance-variation-caused inductance changes, which are mostly due to the stator/rotor slotting effect, and which indirectly represent potential losses generated in the rotor as a result of flux density fluctuations in the rotor core (inducing eddy current losses). Further, these high-order inductance harmonics produce torque ripple, as shown in the paper. Torque ripple, in turn, can cause increased vibration and noise. Therefore, it is important to estimate and verify the actual inductance harmonics caused by slotting effects or some other structural solutions (e.g., winding distribution, rotor pole shape). The paper is organized as follows. The main structural aspects and measurement challenges of ALASynRMs are introduced in Section II. The inductance measurement procedure, theoretical background, and simulations are presented in Section III. Section IV discusses the torque simulations at a standstill with a comparison between the method of virtual work and the inductance measurement procedure. In Section V, the experimental setup and results are presented. Section VI concludes the paper.

II. ALASYNRM STRUCTURE

The ALASynRM is an innovative solution for high-speed applications; it is not yet widely used, but in the academy there is interest in this motor solution [18], [19]. The traditional ALASynRM design involves magnetic and nonmagnetic rotor layers connected with bolts or resin, which mechanically limit the rotor strength and thereby the maximum achievable speed. On the other hand, temperature treatment methods, such as vacuum brazing, hot isostatic pressing, explosion welding, or 3D printing, ensure that, ideally, the rotor behaves like a solid piece of steel from the mechanical point of view, allowing it to reach higher speeds [18]. The motor type has potential to compete with solid-rotor squirrel-cage high-speed induction machines. However, a solid ALA rotor is electrically well conducting (also through the rotor layers that are not galvanically isolated from each other) and can experience strong eddy currents caused by high-order flux density harmonics in the air gap; these harmonics can strongly increase the total losses of the machine [19]. This drawback does not only affect the efficiency of the motor but can pose challenges to the power electronic control of the machine. Further, the very low q-axis inductance and possible time-harmonic-induced eddy currents in the rotor can make the motor control challenging (including effects on the torque and magnetic flux) especially during transients. An example of a solid rotor construction of an ALASynRM is shown in FIGURE 1.

An ALASynRM prototype was built. The stator core and windings of the ALASynRM were directly adopted from a smooth solid-rotor IM [18]. The ALA rotor was manufactured by joining the magnetic and nonmagnetic layers by vacuum brazing. The layers of magnetic structural steel S355 and Inconel 600 were joined by copper brazing and then machined to obtain a cylindrical rotor with a shaft [19]. In this case, the shaft is also made from the same materials (FIGURE 2), because to maximize the saliency ratio, the rotor active part does not provide a hole for a shaft. The shaft implemented in this way does not affect the motor performance. An alternative would be to weld austenitic shafts at the active part ends. The main parameters of the motor are given in Table 1. The stator winding has a short pitching to reduce the flux harmonics and thus the rotor losses and torque ripple.

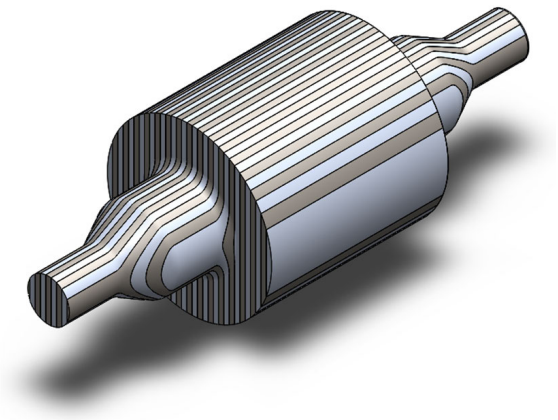

FIGURE 1. Schematic ALASynRM solid rotor made of magnetic and nonmagnetic metal layers.

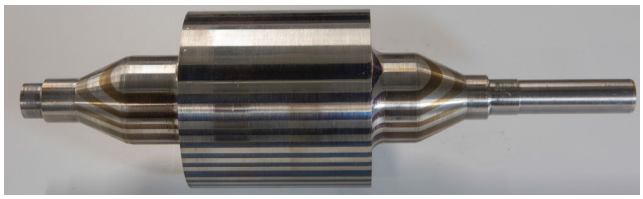

FIGURE 2. Prototype of the ALA rotor.

The manufacturing process is suitable to produce two-pole rotors. Manufacturing of four-pole (or higher number of poles) rotors can, however, be more challenging. It should be noted that rotor ribs, typically used in traditional SynRMs (for the mechanical integrity of the rotor core), are absent in an ALASynRM, making the inductance difference as high as possible. The absence of rotor ribs in an ALASynRM strongly increases the saliency ratio but also air-gap flux harmonics (depending on the number of rotor layers and their thickness). The presence of radial ribs in traditional SynRMs reduces the permeance variation over the rotor periphery, which is not the case in ALASynRMs. High permeance flux density harmonics may cause a high torque ripple of the machine, and thus, require stator skewing, which is not implemented in this case.

Finally, to effectively control the SynRM, the actual synchronous inductances along the d- and q-axes should be known. The AC-supply-based methods used for the classical SynRM to identify synchronous inductance (especially q-axis inductance) at a standstill are not applicable to a solid-rotor ALASynRM because of the high conductivity of the rotor and the strong presence of eddy currents during AC excitation.

III. QUASI-STATIC APPROACH TO INDUCTANCE MEASUREMENT

One of the easiest approaches to measure the inductances is to apply a pulsating current vector through the stator winding along the d- and q-axes and measure the induced voltage. When the resistive voltage drop is known, it is straightforward to estimate the reactive power caused by the machine inductance. However, the presence of a solid rotor or some other damper feature causes significant eddy currents in the rotor during this procedure. These currents induce a flux that opposes the stator-originating flux, and the equivalent measured inductance is much lower than the actual inductance of the machine. A similar situation can occur in a PMSM (caused by eddy currents in the magnets, in a metallic sleeve, or in a solid rotor core) and in an EESM equipped with damper windings.

Another possible approach to measure the synchronous inductance of different SMs with electrically conducting elements in the rotor (including the ALASynRM with a solid rotor) is to rotate the rotor at a synchronous speed at no-load, to apply different voltage values, or use a symmetrical short-circuit (in the case of rotor-excited PMSMs and EESMs) and measure the resulting current [20]. In this case when the stator resistive voltage drop is known, the reactive power caused by the synchronous inductance can be evaluated. However, in this case, only the average (over a complete electrical period) d-axis inductance can be estimated, because at no-load the rotor always tries to align itself along the d-axis. Therefore, measurement of the q-axis inductance and especially the complete inductance variation (at different rotor positions relative to the current vector) is hardly possible. In traditional guidelines, the low-slip test of the EESM aims to give results for the d- and q-axis inductances, but the method is inaccurate and difficult to arrange [21]. Another method is a two-machine approach with a phase shift of 90 degrees at the rated speed. One machine is strongly excited to maintain its d-axis position allowing the d-axis inductance measurement even in saturation, while the other one is used for the q-axis inductance measurement [22].

This paper proposes a new technique for the direct inductance measurement of SMs regardless of whether there is

TABLE 1. Parameters of the 12 kW ALASynRM.

Motor Parameter	Unit	Value
Number of pole pairs		1
Number of stator slots		24
Number of turns in series		24
Number of parallel branches		2
Winding factor		0.925
Short-pitching ratio		5/6
Stator outer diameter	mm	235
Stator inner diameter	mm	100.5
Slot opening width	mm	1.4
Stator length	mm	100
Air-gap length	mm	1
Rotor diameter	mm	98.5
Rated line-to-line voltage	V	225
Connection		delta
Maximum phase current (RMS)	Arms	28.85
Rated frequency	Hz	400
Stator AC resistance at 20°C 400 Hz	mΩ	39
Rotor material	S355/Inconel 600	
Stator material	NO20-13	

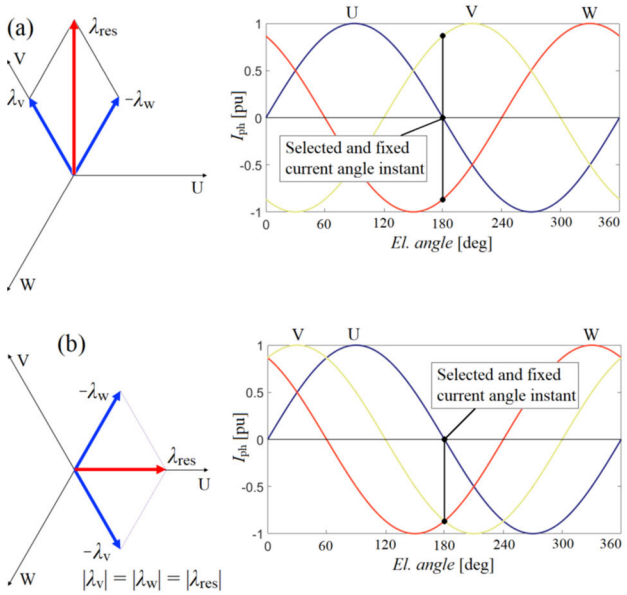

FIGURE 3. Current linkage vectors and the selected current phase angle (resulting in a zero current in phase U) when the current with inappropriate (a) and appropriate (b) polarity is applied to phases V and W.

a solid electrically conducting element in the rotor or not. These inductance data can be used for torque model computation, the results of which give similar motor performance characteristics (including mean torque and torque ripple) as would be directly measured by a torque transducer with a coupled load if stable operation with e.g., 1 Hz or lower can be reached. To verify the accuracy of the proposed method, a direct torque measurement of an ALASynRM is also implemented in this work (including torque ripple measurements) and compared with the torque results obtained from the measured inductance.

The well-known technique for the measurement of inductances in a synchronous reluctance machine that mainly operates at a standstill [23], [24], [25], [26], [27] or with PWM modulation [28] cannot be applied to solid-rotor machines. The main reason is the effect of eddy currents in the rotor that produce a flux opposing the stator alternating flux. The first method of measuring the inductance of a SynRM at a standstill is to inject an alternating current to the stator winding and employ the SynRM model to estimate the fluxes and thus, the inductances. When a stator current is injected at a certain frequency, a pulsating or rotating flux (depending on the connection circuit) is produced. Because the rotor is at a standstill, the pulsating or rotating stator flux is not synchronous with the rotor. This effect is present in both machine types: in a typical transversely laminated rotor SynRM and a solid-rotor ALASynRM. In the latter case, however, the flux variation induces strong eddy currents in the rotor. In a solid rotor, this current can be very high because of the low resistance of the rotor steel. This leads to a reduction in the flux penetrating the rotor with a consequential reduction in the measured inductance (whose value does not correspond to the actual synchronous inductance value). These effects are less evident with a decreasing frequency, and therefore, for the inductance measurements, it is, in principle, possible to apply currents that produce a rotating or pulsating flux with a very low frequency. However, in techniques that include the adoption of PWM modulation, the current is not sinusoidal, and its harmonics can produce eddy currents in the rotor with a consequential increase in losses and deviations in the measurements. Further, even if the PWM modulation is properly filtered, a low supply frequency will lead to a low reactive power, which may be challenging to detect accurately, especially when the same circuit is used both for current supply and detection of reactive power [29]. This can be explained by the different order of the total supply power value and (separated from it) the reactive power value. To minimize the impact of harmonics (as in the case of a nonfiltered PWM supply) and improve the precision of the measurements (when a low-frequency sinusoidal current supply is used), a modified method for the synchronous inductance quasi-static measurement of SMs with a solid conducting element in the rotor is required.

A. THEORETICAL APPROACH

The idea for the inductance measurement of this machine type is based on the vector approach. As shown in FIGURE 3, by considering a three-phase current supply to phases U, V, and W it is possible to select such a current phase angle at which the current in one phase (e.g., U) reaches zero and the total current linkage is generated by only two phases (e.g., V and W). Selection and fixing this current phase angle (when there is no current in one of the phases) allow to manipulate with the currents in only two phases to identify the synchronous inductance.

The traditional three-phase configuration (star connection) cannot, however, be employed in the implementation of the current supply suitable for inductance measurement because, as shown in FIGURE 3a, when supplying two phases (V positive and W negative), the resultant flux is in the quadrature direction with respect to the third phase (U). In this condition, the flux cannot be detected by the third phase. Therefore, in order to have the produced flux linkage in the same direction as the third phase, the polarity of one of the phases must be changed (this requires some manipulation in the winding configuration or in the supply mode), as shown in FIGURE 3b. To achieve this, the motor must have all the winding ends at the terminal box or an access to the star point.

In this case, the resultant current vector and, consequently, the flux vector are different from the original case (owing to the different angles between the phase currents), but this can be taken into account in further manipulations of the measured results to obtain the actual synchronous inductance, as described further.

By analyzing the equations that describe the SynRM model (including flux linkages) it is possible to demonstrate that the main flux produced by the resultant current vector, as shown in FIGURE 3b, is equivalent to the flux produced by the

same current of phase U alone. Starting from the equation of inductances and phase flux linkages [30], considering the presence of currents only in V and W phases (with $I_v = I_w = I$), the equation of the phase U flux linkage can be written as:

$$\psi_u(0, I_v, I_w) = L_{uv} I_v + L_{uw} I_w \quad (1)$$

$$\psi_u(0, I, I) = [-L_{ms} - L_{\Delta s} \cos(2\theta_r)] I \quad (2)$$

where $\psi_u(0, I_v, I_w)$ is the flux linkage produced in phase U by the currents in phases V and W (which makes this flux based on the mutual coupling inductance), L_{uv} is the mutual inductance between phases U and V, L_{uw} is the inductance between phases U and W, L_{ms} is the average air-gap component of the inductance, and $L_{\Delta s}$ is the variable inductance component as a function of rotor position (θ_r).

If current is applied only in phase U, the expression of the flux linkage can be formulated as:

$$\psi_u(I_u, 0, 0) = [L_{\sigma s} + L_{ms} + L_{\Delta s} \cos(2\theta_r)] I_u \quad (3)$$

where $\psi_u(I_u, 0, 0)$ is the phase-U flux linkage, produced by the current running in the same phase. This flux linkage now also includes the leakage component produced in $L_{\sigma s}$, which is the leakage inductance of the phase.

The two expressions (2) and (3) are quite similar to each other, the differences being the sign (when V and W are supplied with an opposite polarity) and the leakage flux of the phase (only present when the flux linkage of the phase is induced and expressed by the current in the same phase).

The model described above includes the first harmonic (inductance variation) only, but it is possible to write the inductances as a Fourier series expansion, thereby obtaining analogous results. For simplicity, only the self-inductance of phase U and one mutual inductance are given. The other inductances have similar expressions according to the phase shift present in the first harmonic model.

$$L_{uu} = L_{\sigma s} + L_{ms} + \sum_{k=2}^{n} [L_{\Delta s,k} \cos(k\theta_r + \varphi_k)] \quad (4)$$

$$L_{uv} = -\frac{1}{2} L_{ms} + \sum_{k=2}^{n} \left[L_{\Delta s,k} \cos\left(k\theta_r + \varphi_k + k\frac{2}{3}\pi \right) \right] \quad (5)$$

where k is the harmonic order, and φ_k is the phase shift of the k-harmonic.

More generally, the model can be represented by a generic function f according to:

$$L_{uu} = L_{\sigma s} + L_{ms} + f(\theta_r) \quad (6)$$

$$L_{uv} = L_{vu} = -\frac{1}{2} L_{ms} + f\left(\theta_r + \frac{2}{3}\pi\right) \quad (7)$$

In this last model, the function f has to be periodic over the observed angle; this can be written with the following consideration:

$$f(\theta_r) + f\left(\theta_r - \frac{2}{3}\pi\right) + f\left(\theta_r + \frac{2}{3}\pi\right) = 0 \quad (8)$$

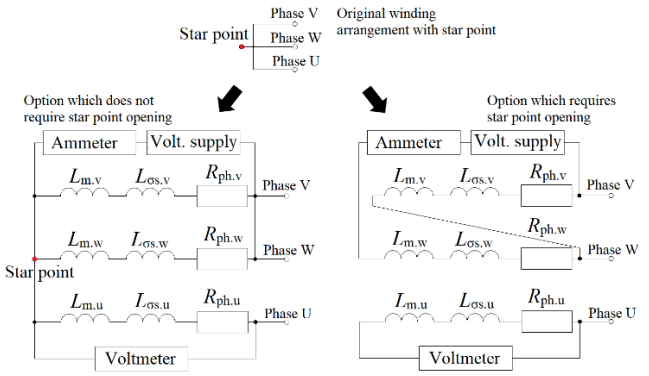

FIGURE 4. Equivalent circuit for inductance measurement.

Considering the supply of (1) for the Fourier series expansion model and the general one, the expression of the phase U flux becomes:

$$\psi_u(0, I, I) = \left[-L_{ms} - \sum_{k=2}^{n} [L_{\Delta s,k} \cos(k\theta_r + \varphi_k)] \right] I \quad (9)$$

$$\psi_u(0, I, I) = [-L_{ms} - f(\theta_r)] I \quad (10)$$

In this model, there is a correspondence between the flux linkage of phase U computed considering the current only in phase U and the flux linkage of phase U computed considering the currents in phases V and W with the same value and sign.

Based on these considerations, it is possible to supply two phases (with the same current and direction) and measure the flux linkage (or the induced voltage) in the third one. From this measurement, the synchronous inductance of the machine can be measured neglecting the leakage inductance (which can be measured by other techniques). This technique separates the circuit of excitation and the measurement circuit, avoiding the influence of the value of the phase resistance or the connection resistance in the measurement results.

The equivalent circuit for the inductance measurement is shown in FIGURE 4. The figure shows that to proceed with the test there is no need for any extra winding or coils, but the existing three-phase winding will suffice without any additional modifications. In a case where the star point should not be opened, the only aspect that must be ensured is the access to all terminals (U, V, W, and the star point) of the machine to rearrange the winding connections (phases V and W and the star point) and voltage measurements between phase U and the star point, as shown in FIGURE 4 (on the left).

However, if the phase resistances deviate significantly from each other (which typically is not the case), then the currents in phases V and W can also deviate in the case of parallel connection through the star point (which does not require opening of the star point). Therefore, to ensure the same currents in phases V and W, a series connection was used in the measurements, which required to open the star point as shown in FIGURE 4 (on the right).

The power supply should apply a quasi-static voltage to minimize the effects of rotor transients, and to compute the flux linkage, a precise flux linkage meter—in practice an induced voltage integrator—is required. The induced voltage e integrator is capable of accurately determining the flux linkage of the system ($\psi = \int e dt$) as it allows all the eddy currents to attenuate after each increment in the exciting current. The circuit is completed with a current measurement in series with phases V and W. The leakage inductance of phase U is present in the modeling, but it remains passive during the test because the current in this phase is negligible.

The measurement can be repeated for different rotor positions to correctly evaluate the variation in the inductance as a function of rotor angle. In this way, it is possible to compute, in addition to the axis inductance, the high-order harmonics of the inductance variation caused by the rotor and stator anisotropic structures. The only drawback of this method is that the stator current linkage waveform stays the same during the measurement. Another deficiency may be that the device (used in the measurements) supplying the measurement current may not be capable of saturating the motor because of the limited supply current values, and therefore, only nonsaturated inductances can be measured. This, however, does not reduce the value of the proposed technique, but is only related to the equipment resources.

B. SIMULATION VERIFICATION

This method was tested in a finite element (FE) simulation environment to verify the reliability of the method by using the Ansys Maxwell software that allows simulating the circuit shown in FIGURE 4 by computing the induced voltage in phase U. By integrating this value it is possible to estimate the flux and compute the inductance. The value of the inductance is that of the previous equations, which neglects the leakage value (because it is based on the mutual magnetic coupling), and it is equal to $[-L_{\mathrm{ms}} - L_{\Delta s} \cos(2\theta_{\mathrm{r}})]$. The computation of the d-axis inductance is carried out with a rotor angle equal to 0 electrical degrees (maximum value of inductance), while the q-axis inductance is obtained with a rotor angle equal to 90 electrical degrees.

The geometry of the simulated machine and the mesh, which consists over 300000 2$^{\mathrm{nd}}$-order elements, are shown in FIGURE 5 and FIGURE 6, respectively. The rotor is composed of 31 layers: 15 of magnetic material and 16 are of nonmagnetic one. The middle layer has a thickness of 6.0 mm, whereas all the other layers have a thickness equal to 3.0 mm. A thicker layer is used in the middle because the highest permeance is found on the d-axis. Further, the brazing interlayers of copper are about 0.1 mm thick or less. The desired rotor diameter of 98.5 mm is achieved with the final milling process. For the load simulation, a very fine mesh must be used to correctly simulate the eddy currents, which occur mostly on the surface of the rotor. For this simulation, a larger mesh size could be employed because these effects can be neglected owing to a very slow flux variation imposed by the proper supply control. Nevertheless,

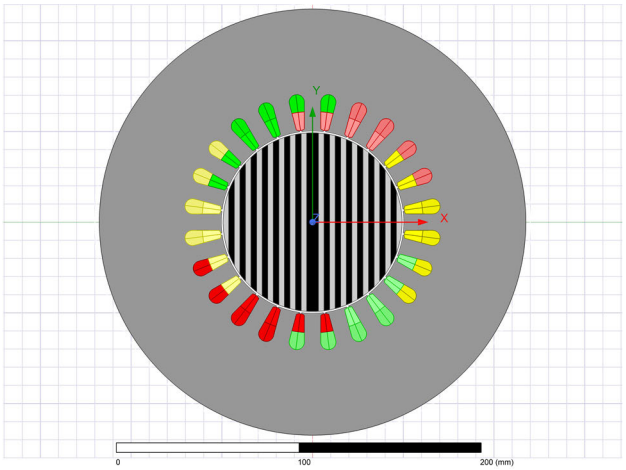

FIGURE 5. ALASynRM geometry under study.

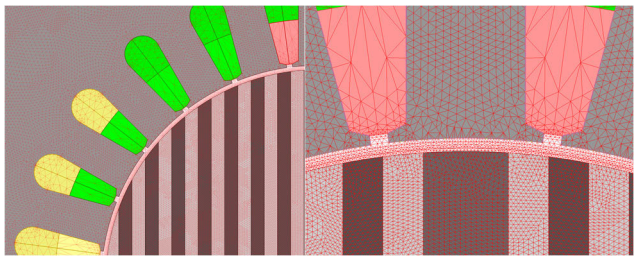

FIGURE 6. Stator and rotor mesh details.

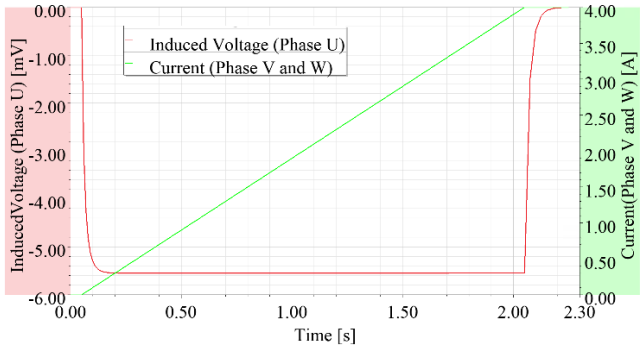

FIGURE 7. Supply current sequence to phases V and W (connected in series) and the induced voltage in phase U.

to achieve comparable results, the same very fine mesh was used.

If the motor is supplied according to the scheme illustrated in FIGURE 4, the rotor (not locked) will be aligned to the equivalent current linkage produced by the stator. In this position, the inductance is equivalent to the d-axis one. FIGURE 6 shows the results in terms of induced voltage (phase U) and supply current sequence (V and W phases). The gradient of the supply voltage is kept equal to 133.33 mV/s to guarantee a quasi-static supply. The current in this simulation reaches the value of 4 A with a maximum gradient of 2 A/s.

Several slope values were investigated, and it was found that up to 10 A/s, the rotor eddy-current effects can be neglected. Above this value, there is a small reduction in the measured inductance. Based on a parametric analysis of all the positions guaranteeing a reasonable simulation time,

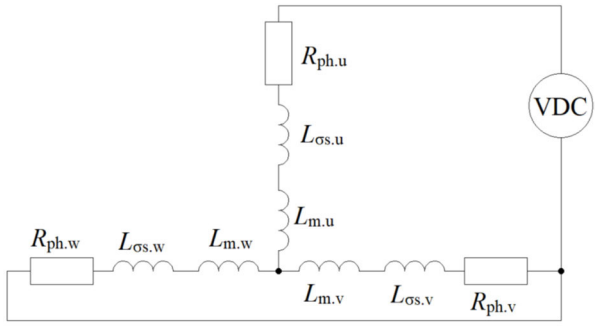

FIGURE 8. Equivalent circuit for the quasi-static torque measurement.

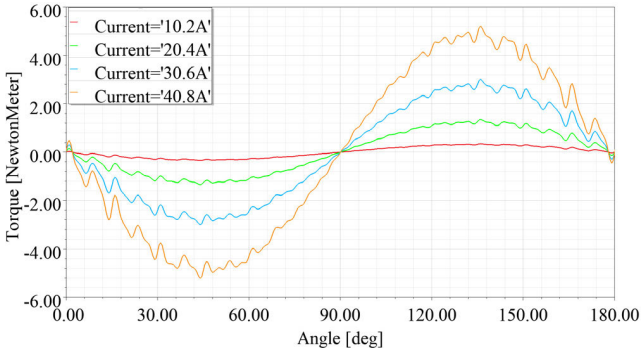

FIGURE 9. Torque computed with the method of virtual work with constant stator currents as a function of rotor angle.

a gradient of 2 A/s was selected for the measurements. In this case, the value can be obtained with a voltage supply gradient of 133.33 mV/s. By integrating the induced voltage it is possible to compute the flux linkage of phase U, and thus, the inductance.

The procedure can be repeated for several rotor positions to obtain the behavior of the inductance as a function of rotor angle (shown in FIGURE 11, Section IV).

From the resultant curve, it is possible to extract the mean value (L_{ms}), the harmonic amplitudes ($L_{\Delta \mathrm{s},k}$), and the harmonic phases (φ_k). To obtain the mutual inductances and the other terms of the inductance matrix it is possible to make a phase shift ($\pm 2/3k\pi$) of the harmonics according to the phase order. The spectrum of the inductance is shown in Section V, where the simulated results are compared with the experimental ones (FIGURE 12).

IV. TORQUE RESULTS

For the torque computation at a standstill, it is possible to supply the motor with a fixed (static in the stator reference frame) stator current vector and slowly vary the rotor position. In this way, it is possible to evaluate the behavior of the torque as a function of rotor position relative to a fixed stator current vector. The equivalent circuit for this measurement is shown in FIGURE 8.

A. SIMULATION RESULTS

Four amplitudes of DC current were applied: the rated current (40.8 A) and 75%, 50%, and 25% of the rated current. The results are shown in FIGURE 9.

From these curves, it is possible to see the high-order harmonic content of the torque mainly caused by the rotor and stator permeance interactions. When the low magnetic reluctance path of the rotor is close to alignment with the current vector (high d-axis current and low q-axis current), the harmonics in the torque are more evident (first and last 45 degrees of the plot). Torque harmonics are lower when the current vector is close to alignment with the high magnetic reluctance path of the rotor (high q-axis current and low d-axis current). The torque in FIGURE 9 is computed by using an FE model, in which the calculation applies nodal forces that are based on the principle of virtual work.

B. INDUCTANCE-BASED APPROACH

By using the definition of inductance and the parametric model, it is possible to compute the torque analytically (for a SynRM) starting from the computation of the magnetic co-energy [31]. The expression is written as

$$T = \frac{p}{2}[I]^T \frac{\mathrm{d}[L]}{\mathrm{d}\theta_{\mathrm{r}}}[I] \tag{11}$$

where p is the number of pole pairs, $[I]$ is the vector of the phase currents, T is the symbol for transposition, and $[L]$ is the inductance matrix.

Considering the first-order model and adopting the Clarke and Park transformations, the expression of torque is written as

$$T = \frac{3}{2}p\left(\psi_{\mathrm{d}} I_{\mathrm{q}} - \psi_{\mathrm{q}} I_{\mathrm{d}}\right) = \frac{3}{2}p\left(L_{\mathrm{d}} - L_{\mathrm{q}}\right) I_{\mathrm{d}} I_{\mathrm{q}} \tag{12}$$

where ψ_{d}, ψ_{q}, L_{d}, L_{q}, I_{d}, I_{q} are the direct and quadrature axis flux linkages, inductances, and currents, respectively.

In the general model, the expression of torque can be written in the UVW model as (13), shown at the bottom of the next page, where f' is the derivative of the generic function, and f is a function of the rotor angle θ_{r}.

If the angle step under consideration is sufficiently low, then the two methods (estimating the torque behavior directly or computing the torque via the estimated inductance) provide similar results.

If the full-order harmonic model is considered, after some manipulation and applying the Clarke and Park transformations, the expression of the torque can be rewritten. Different orders of inductance harmonics present different transformations, and there are three groups with similar transformations:

1) $2j + 6$ (positive direction);
2) $4j + 6$ (negative direction);
3) $6j + 6$ (stationary),

where j is a positive integer.

In this case, the d- and q-axis inductances can be defined in the same way as for the first harmonic order model, but their values do not necessarily represent the maximum and minimum values of the inductance as some high-order harmonics can move the maximum inductance value from the geometrical one. Therefore, the phase shift between the maximum and minimum values can be no larger than 90 degrees.

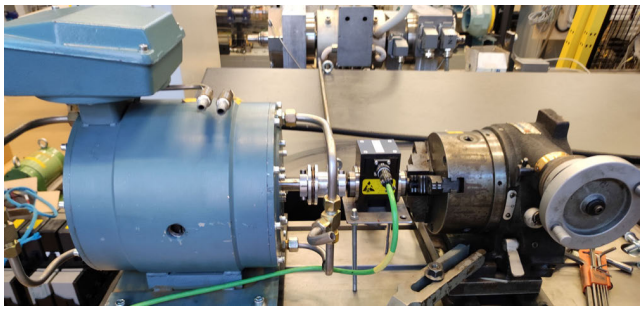

FIGURE 10. Experimental setup.

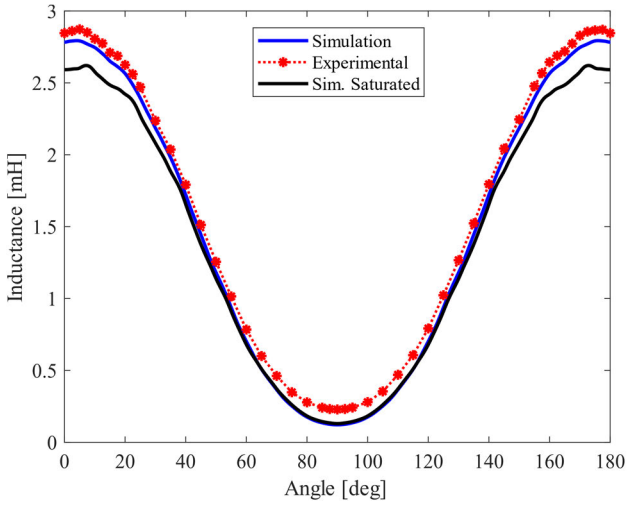

FIGURE 11. Inductance comparison as a function of rotor position.

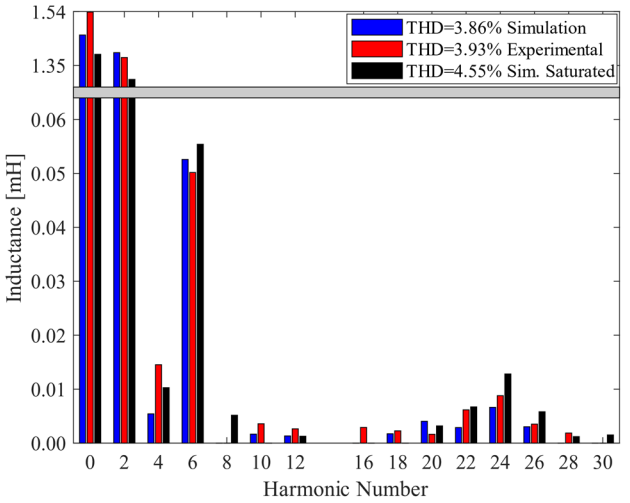

FIGURE 12. Harmonic spectrum comparison of the inductance (the y-axis scale changes at the horizontal gray bar).

V. EXPERIMENTAL RESULTS

The experimental setup includes a division-head gear with a high transmission ratio (90) connected to a motor shaft and a measuring rig for the rotor positioning as shown in FIGURE 10. The connections of the motor windings were modified based on the actual measurement type.

A. INDUCTANCE MEASUREMENT RESULTS AND COMPARISON

For the inductance measurements, the stator windings were connected according to FIGURE 4 (as on the right side), in which the voltage generator was substituted with the excitation circuit of the permeameter AMH-50K-S by Laboratorio Elettrofisico and the voltmeter by the measuring circuit connected to a fluxmeter of the same instrumentation. The fluxmeter has an accuracy of ±0.5% with a resolution from 1 μWb (range 2 mWb) to 100 μWb (range 200 mWb). The power amplifier allows a maximum excitation current of 40 A, which is sufficient in this case. With the permeameter, it is possible to measure the induced voltage in phase U and the input current in phases V and W. By integration, the induced voltage is then converted into the flux linkage of phase U. For the torque measurement, the stator windings were connected as shown in FIGURE 8. The value of the current is adjusted according to the value of the simulation procedure shown in FIGURE 9.

Because of the relatively long-lasting measurement procedure for the flux computation (especially, when a very slow alternating flux is applied not to cause any eddy current reaction on the rotor side), the position of the rotor during these measurements was changed with 2.5° steps close to the d- and q-axes and with 5° steps in other positions. This stepping was selected according to the simulation results, which showed higher inductance fluctuations in the regions close to the d- and q-axes. The results of the inductance measurement compared with the simulated ones are shown in FIGURE 11 and FIGURE 12.

FIGURE 11 and FIGURE 12 show a clear agreement between the simulations and the experiments. The maximum plotted harmonic is fixed to the 30$^{\text{th}}$ because the stepping used for the experimental results limits the possibilities to observe any higher harmonics. Considering the position step applied (5°), these harmonics can exist due to the measurement errors between the different rotor positions, and with this measurement resolution, the 30$^{\text{th}}$ harmonic is the maximum harmonic that can be computed with a reasonable accuracy according to

$$T = \frac{p}{2}\begin{bmatrix} I_{\mathrm{U}} \\ I_{\mathrm{V}} \\ I_{\mathrm{W}} \end{bmatrix}^{T} \begin{bmatrix} f'(\theta_{\mathrm{r}}) & f'\left(\theta_{\mathrm{r}}+\frac{2}{3}\pi\right) & f'\left(\theta_{\mathrm{r}}-\frac{2}{3}\pi\right) \\ f'\left(\theta_{\mathrm{r}}+\frac{2}{3}\pi\right) & f'\left(\theta_{\mathrm{r}}-\frac{2}{3}\pi\right) & f'(\theta_{\mathrm{r}}) \\ f'\left(\theta_{\mathrm{r}}-\frac{2}{3}\pi\right) & f'(\theta_{\mathrm{r}}) & f'\left(\theta_{\mathrm{r}}+\frac{2}{3}\pi\right) \end{bmatrix} \begin{bmatrix} I_{\mathrm{U}} \\ I_{\mathrm{V}} \\ I_{\mathrm{W}} \end{bmatrix} \tag{13}$$

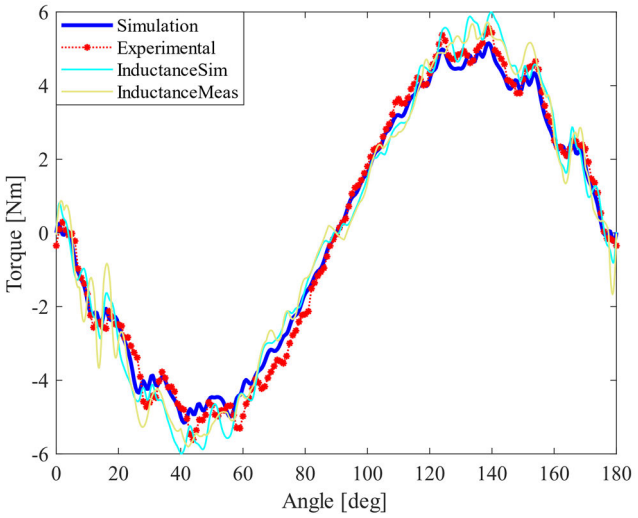

FIGURE 13. Comparison of the simulated and measured torque behaviors as a function of rotor position at the rated current.

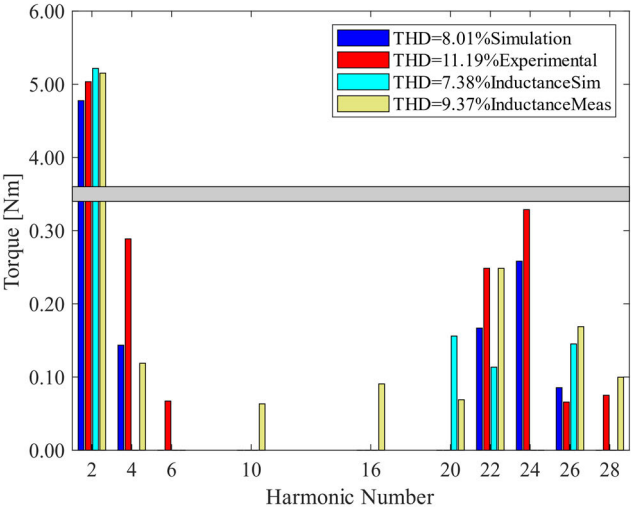

FIGURE 14. Comparison of the simulated and measured torque harmonic spectra at the rated current (the y-axis scale changes at the horizontal gray bar).

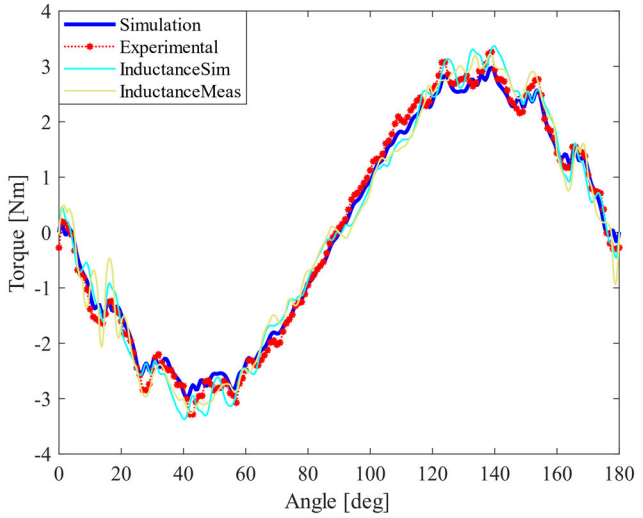

FIGURE 15. Comparison of the simulated and measured torque behaviors as a function of rotor position at 75% of the rated current.

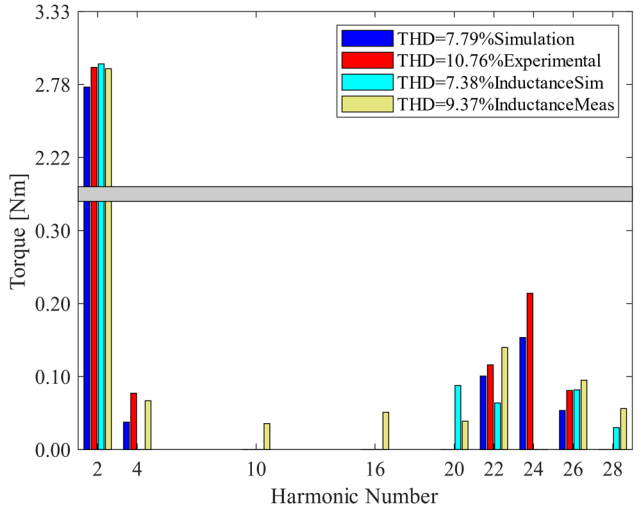

FIGURE 16. Comparison of the simulated and measured torque harmonic spectra at 75% of the rated current (the y-axis scale changes at the horizontal gray bar).

the Nyquist theorem (frequency sampling should be at least two times the detected one or higher).

The low-order harmonics (for example, the 6^{th}, which has a larger value and is more important from the perspective of motor performance) are very similar, which makes the results reliable and applicable for further evaluation of the motor characteristics. The medium-order harmonics (from the 10th to the 26th) mainly exist in the experimental results. The harmonic numbers in FIGURE 12 are computed considering a complete mechanical revolution (360°). Because the inductances are periodic functions with a period of 180°, only even harmonics are present.

The main differences in the harmonic amplitudes are due to several factors: the larger angle step used in the experiments compared with the simulations, deviations in the magnetic properties caused by heat and mechanical treatments, manufacturing tolerances in the layer thickness, end winding effects, and measurement tolerances. However, these differences are quite small and do not affect the proposed results in general.

The motor was designed with a relatively low maximum flux density in the stator yoke and teeth also at the rated current and torque in order to reduce the core losses at high speeds. The inductance measurement was performed by using currents comparable with the motor rated current. For clarity, a simulation with a very high phase current (60 A) was carried out, and the results are shown in FIGURE 11 and FIGURE 12 (Sim. Saturated), in which it is possible to see the saturation effect, with a reduction in the inductance close to zero degrees. There is also a reduction in the mean value, in the second harmonic (the main one), and an increase in the 24^{th} harmonic (the one caused by the slotting effect). The proposed method can incorporate saturation effects for the computation of the phase inductance as a function of relative phase current with several positions to obtain the

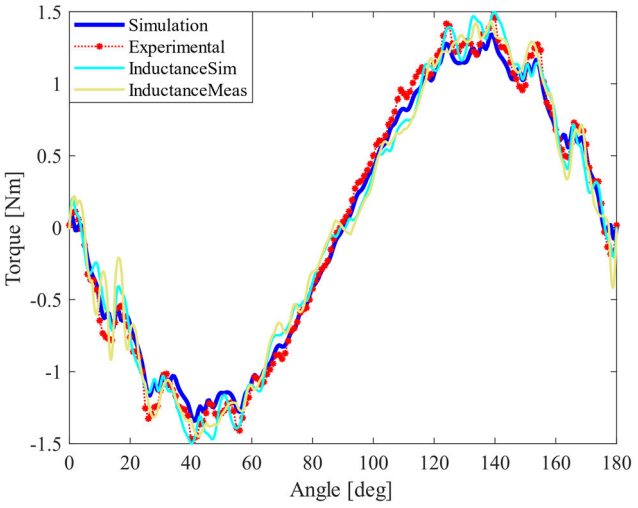

FIGURE 17. Comparison of the simulated and measured torque behaviors as a function of the rotor position at 50% of the rated current.

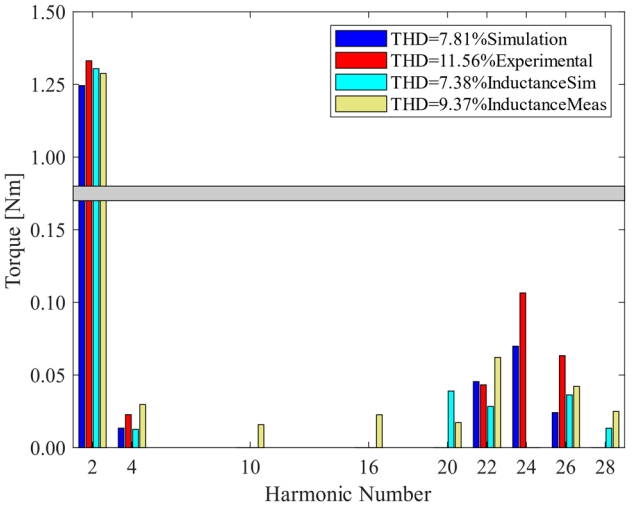

FIGURE 18. Comparison of the simulated and measured torque harmonic spectra at the 50% of the rated current (the y-axis scale changes at the horizontal gray bar).

harmonics. A useful parameter that can also be measured is the axis inductances (d and q) as a function of related currents.

B. TORQUE MEASUREMENT RESULTS AND COMPARISON

The next step is the verification of the torque between the FE simulation results (employing nodal forces that are based on the principle of virtual work), the computation with the simulation and experimental results of the inductance with (14)–(17), as shown at the bottom of the page, and the measurements of the torque directly with the torquemeter. The results are shown in FIGURE 13 to FIGURE 20. The harmonic numbers for these figures are computed considering a complete mechanical revolution (360°).

The experimental results confirm the accuracy of the simulation model for the torque computation using the inductance values. The torque computation applying the inductance model (14)–(17) allows to evaluate most of the torque harmonics with a high accuracy.

Considering the rated peak current (40.8 A), the main harmonic (the second) is around 5 Nm for each method, as expected by the rated torque of the motor. The inductance-based method for the torque computation works correctly, and the higher order harmonics from the simulations (blue and cyan) and from the experiments (red and gold) have similar orders and values.

Both in the experimental tests and simulations, the main harmonics are located around the 24^{th} harmonic. Similar results were obtained for the other current values: 75%, 50%, and 25% of the rated one. The results of these curves are quite similar to the one obtained at the rated current.

The torque harmonics computed with the inductance-based model present similar THDs and similar ratios between the amplitudes of harmonics. The THD coefficients obtained by the FEM simulations and the experimental results have slightly different values with the variation of current. Therefore, the experimental torque measurements and the simulations confirm the validity of the proposed method.

By comparing FIGURE 12, FIGURE 14, FIGURE 16, FIGURE 18, and FIGURE 20 it can be seen that the higher order inductance harmonics (the 20^{th}-28^{th}) have lower amplitudes compared with the lower harmonics (the fourth) but produce higher torque amplitude harmonics. This is explained by the equations and the derivative relation between torque and inductance. With this method, the sixth harmonic and its multiple torque harmonics are not visible because in a rotating machine they are produced by the trav-

$$\text{If } k = 2j + 6T_k = \frac{3}{4}p\begin{bmatrix} I_\text{d} & I_\text{q} \end{bmatrix}\begin{bmatrix} -L_{\Delta s,k}\sin\left[(k-2)\,\vartheta_\text{r} + \psi_k\right] & L_{\Delta s,k}\cos\left[(k-2)\,\vartheta_\text{r} + \psi_k\right] \\ L_{\Delta s,k}\cos\left[(k-2)\,\vartheta_\text{r} + \psi_k\right] & L_{\Delta s,k}\sin\left[(k-2)\,\vartheta_\text{r} + \psi_k\right] \end{bmatrix}\begin{bmatrix} I_\text{d} \\ I_\text{q} \end{bmatrix} \tag{14}$$

$$\text{if } k = 4j + 6T_k = \frac{3}{4}p\begin{bmatrix} I_\text{d} & I_\text{q} \end{bmatrix}\begin{bmatrix} -L_{\Delta s,k}\sin\left[(k+2)\,\vartheta_\text{r} + \psi_k\right] & -L_{\Delta s,k}\cos\left[(k+2)\,\vartheta_\text{r} + \psi_k\right] \\ -L_{\Delta s,k}\cos\left[(k+2)\,\vartheta_\text{r} + \psi_k\right] & L_{\Delta s,k}\sin\left[(k+2)\,\vartheta_\text{r} + \psi_k\right] \end{bmatrix}\begin{bmatrix} I_\text{d} \\ I_\text{q} \end{bmatrix} \tag{15}$$

$$\text{if } k = 6j + 6T_k = 0 \text{ with } j = 0, 1, 2, \ldots, N \tag{16}$$

$$T = \frac{3}{2}\left(L_\text{d} - L_\text{q}\right) I_\text{d} I_\text{q} + \sum_{k=4}^{N} T_k \tag{17}$$

$$L_\text{d} = L_\mu + L_{\Delta s,2} L_\text{q} = L_\mu - L_{\Delta s,2} \tag{18}$$

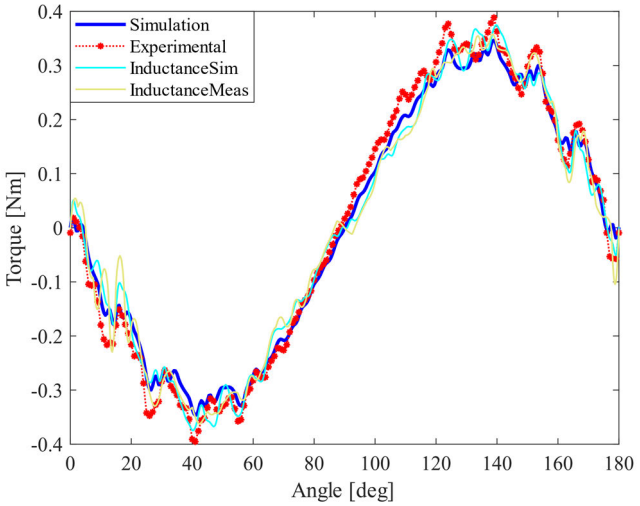

FIGURE 19. Comparison of the torque behaviors as a function of rotor position at 25% of the rated current.

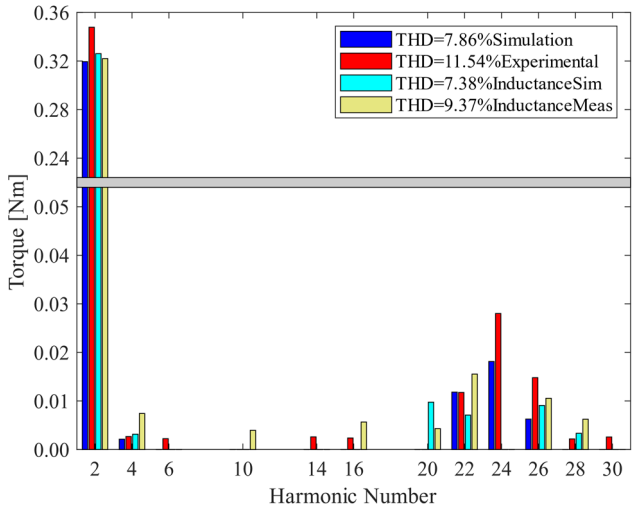

FIGURE 20. Comparison of the simulated and measured harmonic spectra at 25% of the rated current (the y-axis scale changes at the horizontal gray bar).

eling fifth and seventh stator current linkage harmonics. As in this measurement the current linkage is not traveling but it is stationary, the phases of the stator fundamental and high-order harmonics do not change, and therefore, we do not see the sixth torque harmonic in the results. The technique can measure the harmonics of the mutual terms of the inductance, and the self-inductance is computed by phase shifting. In this way, some effects on the self-inductance and on the torque ripple are neglected.

VI. CONCLUSION

A novel methodology of the synchronous inductance measurement of SMs was verified with an ALASynRM. It was shown that even if the rotor is completely made of a solid electrically conducting body, it is possible to measure the inductance of a motor at a standstill and at any rotor position. The measured inductance matched well the estimated inductance obtained by the FE simulation, except for some high-order harmonics. A slight difference in the harmonic amplitudes can be explained by the large angle step in the inductance measurement, the deviation of magnetic properties caused by heat and mechanical treatments, manufacturing tolerances in the layer thickness, end-winding effects, and measurement tolerances. However, the spectra of the inductance harmonics match well, which can already give an understanding of the main motor parameters.

In order to validate the approach further, inductance measurements as a function of rotor position were simulated and tested. In this way, in addition to the d- and q- axis inductances, it is possible to compute the inductance harmonics. From the analytical expression of torque obtained by applying the harmonic model of the inductance, it is possible to compute the torque with a fixed stator current vector and different rotor positions. The computed torque was compared with the experimental one for different current values. The comparison shows a good agreement between the obtained results, confirming the validity of the proposed approach.

The drawbacks of the proposed method are the need to use the phase shift technique to compute the inductance matrix terms, which results in neglecting the additional effects in the torque ripple computation; however, the approach for the torque ripple is valid when considering a fixed current linkage. The measured value of the inductance does not include the leakage inductance. Still, for a rotating field, the harmonics produced by the windings must be introduced; this can be addressed in further developments. Future works could also investigate the opportunity to evaluate the cross-saturation effects in the inductance computation with the proposed method.

REFERENCES

[1] M. Chowdhury, A. Tesfamicael, M. Islam, and I. Husain, "Design optimization of a synchronous reluctance machine for high-performance applications," *IEEE Trans. Ind. Appl.*, vol. 57, no. 5, pp. 4720–4732, Sep. 2021.

[2] A. Credo, G. Fabri, M. Villani, and M. Popescu, "Adopting the topology optimization in the design of high-speed synchronous reluctance motors for electric vehicles," *IEEE Trans. Ind. Appl.*, vol. 56, no. 5, pp. 5429–5438, Sep. 2020.

[3] G. Du, Q. Zhou, S. Liu, N. Huang, and X. Chen, "Multiphysics design and multiobjective optimization for high-speed permanent magnet machines," *IEEE Trans. Transport. Electrific.*, vol. 6, no. 3, pp. 1084–1092, Sep. 2020.

[4] A. Fatemi, T. W. Nehl, X. Yang, L. Hao, S. Gopalakrishnan, A. M. Omekanda, and C. S. Namuduri, "Design optimization of an electric machine for a 48-V hybrid vehicle with comparison of rotor technologies and pole-slot combinations," *IEEE Trans. Ind. Appl.*, vol. 56, no. 5, pp. 4609–4622, Sep. 2020.

[5] G. Bramerdorfer, G. Lei, A. Cavagnino, Y. Zhang, J. Sykulski, and D. A. Lowther, "More robust and reliable optimized energy conversion facilitated through electric machines, power electronics and drives, and their control: State-of-the-art and trends," *IEEE Trans. Energy Convers.*, vol. 35, no. 4, pp. 1997–2012, Dec. 2020.

[6] A. Credo, G. Fabri, M. Villani, and M. Popescu, "A robust design methodology for synchronous reluctance motors," *IEEE Trans. Energy Convers.*, vol. 35, no. 4, pp. 2095–2105, Dec. 2020.

[7] G. Lei, G. Bramerdorfer, B. Ma, Y. Guo, and J. Zhu, "Robust design optimization of electrical machines: Multi-objective approach," *IEEE Trans. Energy Convers.*, vol. 36, no. 1, pp. 390–401, Mar. 2021.

[8] L. Aarniovuori, J. Kolehmainen, A. Kosonen, M. Niemela, H. Chen, W. Cao, and J. Pyrhonen, "Application of calorimetric method for loss measurement of a SynRM drive system," *IEEE Trans. Ind. Electron.*, vol. 63, no. 4, pp. 2005–2015, Apr. 2016.

[9] L. Aarniovuori, H. Karkkainen, M. Niemela, K. Cai, J. Pyrhonen, and W. Cao, "Experimental investigation of the losses and efficiency of 75 kW induction motor drive system," in *Proc. IECON 45th Annu. Conf. IEEE Ind. Electron. Soc.*, Oct. 2019, pp. 1052–1058.
[10] I. Petrov, P. Lindh, M. Niemelä, E. Scherman, and J. Pyrhönen, "High-torque-density IPMSM rotor pole geometry adjustment for smooth torque," *IEEE Access*, vol. 7, pp. 52650–52658, 2019.
[11] A. Credo, M. Villani, M. Popescu, and N. Riviere, "Application of epoxy resin in synchronous reluctance motors with fluid-shaped barriers for E-mobility," *IEEE Trans. Ind. Appl.*, vol. 57, no. 6, pp. 6440–6452, Nov. 2021.
[12] S.-B. Jun, C.-H. Kim, J. H. Lee, J.-K. Kang, Y.-J. Kim, and S.-Y. Jung, "Parameter optimization for reducing torque ripple and harmonic losses of multi-layered interior permanent-magnet synchronous motors," *IEEE Access*, vol. 10, pp. 10536–10552, 2022.
[13] I. Petrov, P. Ponomarev, S. Shirinskii, and J. Pyrhonen, "Inductance evaluation of fractional slot permanent magnet synchronous motors with non-overlappingwinding by analytical approaches," in *Proc. 16th Eur. Conf. Power Electron. Appl.*, Aug. 2014, pp. 1–10.
[14] P. Ponomarev, I. Petrov, and J. Pyrhonen, "Influence of travelling current linkage harmonics on inductance variation, torque ripple and sensorless capability of tooth-coil permanent-magnet synchronous machines," *IEEE Trans. Magn.*, vol. 50, no. 1, pp. 1–8, Jan. 2014.
[15] C. Candelo-Zuluaga, J.-R. Riba, and A. Garcia, "PMSM torque-speed-efficiency map evaluation from parameter estimation based on the stand still test," *Energies*, vol. 14, no. 20, p. 6804, Oct. 2021.
[16] G. Li, Z. Wu, S. Han, F. Jiang, T. Yang, and G. Wang, "Modified AC standstill method for PMSM d - q axis inductances measurement," *IET Sci., Meas. Technol.*, vol. 14, no. 4, pp. 430–434, Jun. 2020.
[17] H. B. Ertan and I. Sahin, "Evaluation of inductance measurement methods for PM machines," in *Proc. 20th Int. Conf. Electr. Mach.*, Sep. 2012, pp. 1672–1678.
[18] V. Abramenko, I. Petrov, J. Nerg, and J. Pyrhonen, "Synchronous reluctance motors with an axially laminated anisotropic rotor as an alternative in high-speed applications," *IEEE Access*, vol. 8, pp. 29149–29158, 2020.
[19] V. Abramenko, J. Nerg, I. Petrov, and J. Pyrhonen, "Influence of magnetic and nonmagnetic layers in an axially laminated anisotropic rotor of a high-speed synchronous reluctance motor including manufacturing aspects," *IEEE Access*, vol. 8, pp. 117377–117389, 2020.
[20] V. Rallabandi, N. Taran, D. M. Ionel, and P. Zhou, "Inductance testing for IPM synchronous machines according to the new IEEE std 1812 and typical laboratory practices," *IEEE Trans. Ind. Appl.*, vol. 55, no. 3, pp. 2649–2659, May/Jun. 2019.
[21] O. Sugiura and Y. Akiyama, "Precise method for measuring Xd and Xq based on slip test of synchronous machines," in *Proc. Conf. Rec. IEEE Ind. Appl. Conf. 28th IAS Annu. Meeting*, Oct. 1993, pp. 155–162.
[22] W. Nürnberg and R. Hanitsch, *Die Prüfung Elektrischer Maschinen*. Berlin, Germany: Springer-Verlag, 1987.
[23] Y. Gao, R. Qu, and Y. Liu, "An improved AC standstill method for inductance measurement of interior permanent magnet synchronous motors," in *Proc. Int. Conf. Electr. Mach. Syst. (ICEMS)*, Oct. 2013, pp. 927–931.
[24] Y. Gao, R. Qu, Y. Chen, J. Li, and W. Xu, "Review of off-line synchronous inductance measurement method for permanent magnet synchronous machines," in *Proc. IEEE Conf. Expo. Transp. Electrific. Asia–Pacific (ITEC Asia–Pacific)*, Aug. 2014, pp. 1–6.
[25] S. A. Odhano, R. Bojoi, S. G. Rosu, and A. Tenconi, "Identification of the magnetic model of permanent-magnet synchronous machines using DC-biased low-frequency AC signal injection," *IEEE Trans. Ind. Appl.*, vol. 51, no. 4, pp. 3208–3215, Jul. 2015.
[26] S.-H. Hwang, J.-M. Kim, H. V. Khang, and J.-W. Ahn, "Parameter identification of a synchronous reluctance motor by using a synchronous PI current regulator at a standstill," *J. Power Electron.*, vol. 10, no. 5, pp. 491–497, Sep. 2010.
[27] M. Hinkkanen, P. Pescetto, E. Molsa, S. E. Saarakkala, G. Pellegrino, and R. Bojoi, "Sensorless self-commissioning of synchronous reluctance motors at standstill without rotor locking," *IEEE Trans. Ind. Appl.*, vol. 53, no. 3, pp. 2120–2129, May 2017.
[28] R. Raja, T. Sebastian, and M. Wang, "Online stator inductance estimation for permanent magnet motors using PWM excitation," *IEEE Trans. Transport. Electrific.*, vol. 5, no. 1, pp. 107–117, Mar. 2019.
[29] H. Hamalainen, J. Pyrhonen, J. Nerg, and J. Talvitie, "AC resistance factor of litz-wire windings used in low-voltage high-power generators," *IEEE Trans. Ind. Electron.*, vol. 61, no. 2, pp. 693–700, Feb. 2014.
[30] I. Boldea, *Reluctance Synchronous Machines and Drives*. Oxford, U.K.: Clarendon Press, 1996.
[31] D. Brown and E. P. Hamilton, "Electromechanical energy conversion," in *Electromechanical Motion Devices*. New York, NY, USA: Macmillan, 1984, pp. 49–95.

ANDREA CREDO received the B.Sc. and M.Sc. degrees (Hons.) in electrical engineering and the Ph.D. degree (cum laude) from the University of L'Aquila, L'Aquila, Italy, in 2015, 2017, and 2021, respectively. His research interest includes the design and the control of synchronous reluctance motor. He received the ICEM Jorma Luomi Student Forum Award from the ICEM 2020 in Gothenburg, Sweden (Virtual Conference).

ILYA PETROV received the D.Sc. degree in electrical engineering from the Lappeenranta University of Technology (LUT), Lappeenranta, Finland, in 2015. He is currently a Fellow Researcher with the Department of Electrical Engineering, LUT.

VALERII ABRAMENKO received the Specialist degree in electrical drives and automation of industrial installations from South Ural State University (SUSU), Chelyabinsk, Russia, in 2014, and the Master of Science degree in electrical engineering jointly from SUSU and the Lappeenranta University of Technology (LUT), Lappeenranta, Finland, in 2017.

He is currently a Researcher at the Department of Electrical Engineering, LUT. His research interest includes high-efficient synchronous motors.

JUHA PYRHÖNEN (Senior Member, IEEE) was born in Kuusankoski, Finland, in 1957. He received the D.Sc. degree in electrical engineering from the Lappeenranta University of Technology (LUT), Lappeenranta, Finland, in 1991. He became a Professor of electrical machines and drives with LUT in 1997. He is engaged in research and development of electric motors and power-electronic-controlled drives. He is currently researching a new carbon-based materials for electrical machines. His research interests include development of special electric drives for distributed power production, traction, and high-speed applications, and permanent magnet materials and applying them in machines.

Open Access funding provided by 'Università degli Studi dell'Aquila' within the CRUI CARE Agreement